AIAA AVIATION Forum
5-9 June 2017, Denver, Colorado
23rd AIAA/CEAS Aeroacoustics Conference

10.2514/6.2017-3865

Applicability of Early Acoustic Theory for Modern Propeller Design

Mark T. Kotwicz Herniczek* and Daniel Feszty†
Carleton University, Ottawa, ON, Canada

Sid-Ali Meslioui‡ and Jong Park§
Pratt & Whitney Canada, Longueuil, QC, Canada

The relevance of several computationally-inexpensive acoustic methods is evaluated for use in modern propeller design. The acoustic models considered predict far-field harmonic noise. They range in complexity from a direct implementation of the equations derived by Gutin and Deming to Hanson's helicoidal surface theory of propellers. The advantage of these acoustic models is that they do not require chord-wise aerodynamic data and therefore do not need to be coupled to a panel or grid-based aerodynamic solver. Each implemented method is compared to fourteen test cases originating from nine separate published acoustic experiments. The experimental data considered encapsulates a range of propeller geometries, blade numbers, microphone locations, tip speeds, and forward Mach speeds. Limited acoustic results are also produced using the Ffowcs Williams-Hawkings equation, coupled to a panel method and grid-based computational fluid dynamics solver, in order to quantify the accuracy of the selected methods relative to current, more sophisticated techniques. The implemented acoustic models demonstrate good agreement with the experimental data, particularly for the prediction of the maximum tonal noise for which the model based on Hanson's work has an average error of 7.2 dB. The computationally-inexpensive models show better agreement with experimental data compared to those coupling the FW-H equation to aerodynamic solvers. The presented results suggest that the implemented acoustic methods, and the model based on Hanson's work in particular, remain a valuable resource for propeller noise prediction, especially for design and optimization studies, where a low runtime is important.

Nomenclature

A_x	airfoil cross-sectional area, approximated as $0.6853bh$, m^2
B	number of blades
D	propeller diameter, m
$J_{mB}(x)$	Bessel function of order mB and argument x
M	forward speed or freestream Mach number
MCA	mid-chord aligment, m
M_s	section relative Mach number, $\sqrt{M^2 + r^2 M_t^2}$
M_t	tip Mach number, $\Omega r_t / c$
P_0	reference sound pressure, 2×10^{-5} Pa
P_{m_L}, P_{m_T}	root mean square sound pressure (loading and thickness component), Pa
R	radial distance along propeller blade, m
S	observer distance from propeller hub, $\sqrt{x^2 + y^2 + z^2}$, m
S_0	amplitude radius, $\sqrt{x^2 + (1 - M^2)Y^2}$, m

*MASc Candidate, Department of Mechanical and Aerospace Engineering.
†Associate Professor, Department of Mechanical and Aerospace Engineering, AIAA Member.
‡Manager and Technical Fellow, Acoustics.
§Senior Engineer, Acoustics.

S_r, θ_r	distance, S, and angle, θ, in retarded reference frame, m, rad
Y	observer distance from propeller axis, $\sqrt{y^2 + z^2}$, m
b	blade chord, m
c	speed of sound, m/s
dQ	discretized propeller torque, Nm
dT	discretized propeller thrust, N
h	maximum airfoil thickness, m
k_x	wave number
m	harmonic number
r	non-dimensional radial distance along propeller blade, R/r_t
r_t	propeller tip radius, $D/2$, m
x, y, z	observer coordinates relative to propeller hub, m
Ω	propeller angular velocity, rad/s
Ψ_L, Ψ_V	normalized loading and thickness source transforms
α	pitch angle of propeller shaft axis relative to flight direction, rad
ϕ	tangential angle, $\arctan(z/y)$, rad
ϕ_s	phase lag due to sweep, rad
ϕ_t	blade twist angle relative to propeller plane, rad
ρ	air density, kg/m^3
θ	observer angle relative to flight direction, $\arccos(x/S)$, rad
θ'_r, ϕ'	angles θ_r and ϕ relative to propeller shaft axis, rad

I. Introduction

THE acoustic signature of commercial propeller aircraft is becoming a key design parameter as airlines shift from turbofan to turboprop engines for short-duration flights[1,2] and restrictions on the noise pollution surrounding airports become more stringent. The new International Civil Aviation Organization (ICAO) noise standard in Annex 16 Vol. 1, Chapter 14 constitutes a 7 dB increase in stringency of the Effective Perceived Noise Level (EPNdB) and will apply to propeller aircraft under 55 tonnes in 2020.[3] Propeller aircraft noise also has a direct impact on passenger comfort and on the health of those living or working near airports.[4,5] While small propeller aircraft produce negligible noise, there is concern relating to in-flight cabin noise and community noise for larger propeller aircraft, particularly for the high efficiency prop-fan which operates at supersonic helical tip speeds.[6,7] As such, propeller noise testing and prediction are active fields of research.

Noise predictions methods are typically grouped into two categories: frequency-domain methods and time-domain methods. Time-domain methods retain the pressure time history and allow the propeller geometry to be treated with superior precision. However, they require the computation of retarded blade locations and need high quality aerodynamic data to obtain accurate results, particularly if the propeller experiences supersonic flow.[8] Frequency-domain methods eliminate time as a variable by taking the Fourier transform of the wave equation. For this reason, the pressure time history and some information regarding the propeller geometry is lost, however, acoustic results are generally not affected up to a fairly high order.[8] Frequency-domain methods are less computationally expensive and have the advantage of being more explicit as to the effects of different parameters on the predicted noise. Modern prediction methods typically require chord-wise pressure or loading data, however, for design or optimization studies, it is often preferable to approximate the chord-wise terms in favor of lower runtimes.

The first successful acoustic theory was developed by Gutin in 1936 when he represented the steady aerodynamic forces on the propeller as a ring of acoustic dipole sources acting at a certain effective radius.[9] Gutin's theory, however, was limited to loading noise for propellers with axial flow, simple geometry, low tip speed and no forward speed. Since then there have been significant advances in acoustic theory due to the work of many researchers who have removed these limitations.[10–17] A thorough review of propeller noise prediction methodology, detailing these advances, has been published by multiple authors, including Morfey,[18] Magliozzi,[8,19] Farassat,[20] and Metzger.[21]

In reviewing the literature, a large number of acoustic models were found, however, a significant number lacked sufficient validation to experimental data. This same observation was made by Metzger, who also noted that "needs in propeller prediction are not more methods, but a consolidation of the unique features of the

many existing methods" and called for a comprehensive evaluation of existing methods to well documented, high quality data.[21] Thorough validation using multiple test cases is essential due to the significant noise level variation based on microphone location and the measurement fluctuations seen in some acoustics experiments. One such experiment, performed by Soderman and Horne, saw variations of up to 10 dB for the first harmonic in identical runs.[22] Although the implemented methods have been compared to experiment, there lacks a comprehensive validation study using multiple experiments with a range of propeller geometries and operational conditions.

This paper investigates the relevance of several analytical models originating from the work of Gutin and Deming for far-field harmonic noise prediction across a wide range of propeller configurations, including the modern, high speed prop-fan. Results for a portion of the selected test cases are compared to a panel method (SmartRotor) and a grid-based computational fluid dynamics method (STAR-CCM+), coupled to the Ffowcs Williams-Hawkings (FW-H) equation, to establish the relative accuracy of the implemented models.

II. Aerodynamic and Acoustic Prediction Methods

Acoustic models were selected based on their computational cost, with the desired runtime on a standard desktop computer of less than one second. This criteria severely restricted the complexity of aerodynamic solvers and ruled-out the implementation of models based on the FW-H equation. Frequency-domain methods were selected due their low computational cost, lower sensitivity to input error and ease of use. Therefore, the acoustic models investigated originate primarily from the work of Gutin, Deming and Hanson due to their minimal need for aerodynamic data. To allow for variable blade geometry without significantly increasing computation time, Blade Element Momentum Theory (BEMT) was implemented to obtain discretized values for thrust and torque along the propeller blade. An additional benefit of the chosen acoustic models is their white-box nature, where the influence of parameters is clear and the user does not need to be concerned with tuning or convergence parameters, thus eliminating a possible source of error.

Two sophisticated acoustic models were also selected to evaluate the accuracy of the aforementioned models relative to more complex techniques. Both utilize the Farassat 1A formulation of the FW-H equation[17] and differ primarily on the coupled aerodynamic solver. The first utilizes an in-house vortex particle-based Computational Fluid Dynamics (CFD) code called SmartRotor which combines a potential-flow panel method for the lifting surfaces with a Lagrangian vortex particle model to capture the wake.[23,24] The second uses STAR-CCM+, a grid-based commercial CFD code to obtain aerodynamic data with an Unsteady Reynolds-Averaged Navier-Stokes (URANS) simulation.[25] Validation of the latter two methods are detailed in Ref. 23 and Ref. 25, respectively. It should be noted that these two prediction methods were not implemented by the author, but rather by Boots and Hambrey, who used some of the same experiments presented in this paper as validation cases. An overview of these two methods, alongside details of the simulation setup for the results included in this paper, is presented in Ref. 26. As such, this paper will not go into further detail regarding either of these two prediction methods.

A summary of the acoustic prediction methods used to obtain the results presented in this paper is given in Table 1. It should be noted that the computational times listed in the table were not normalized and represent runtimes on two separate platforms. Smartrotor and the frequency-domain methods were run on a six processor desktop computer, while STAR-CCM+ runs were performed on a cluster of forty processors.

II.A. Aerodynamic Prediction

Blade Element Momentum Theory (BEMT) was used to obtain a discretized thrust and torque distribution for each of the implemented prediction models. Since BEMT is a standard method for propeller design, only a brief description is provided.

II.A.1. Blade Element Momentum Theory

BEMT is a hybrid method which combines principles from both blade element theory and momentum theory. Blade Element Theory (BET), discretizes the propeller such that each finite element can be considered as a two-dimensional airfoil for which aerodynamic forces and moments can be determined. Momentum theory, on the other hand, applies conservation of mass, momentum and energy to a control volume surrounding the propeller and serves to provide BET with an approximation of the inflow velocity. By dividing the propeller into discrete elements, radial variation in twist, chord length and airfoil shape is permitted.

Table 1. Acoustic Prediction Methods.

Method Name	Acoustic Prediction Capability				Computational Time Scale	Test Cases Considered*
	Forward Flight	Sweep	Non-compactness	Non-axial Flow		
Gutin and Deming	No	No	No	No	Seconds‡	1–14
Barry and Magliozzi	Yes	No	No	No		
Hanson	Yes	Yes	Yes	Limited†		
SmartRotor	Yes				Hours	1–2
STAR-CMM+	Yes				Days	1–3

* test case numbering refers to the numbering in Table 2

† flow angle had a minimal impact on prediction results

‡ the current implementation, coded in Python 3, can process approximately 100 test cases in 1 second

Two variations of BEMT were used; the first is a direct implementation of Ref. 27, while the second was implemented from Refs. 28 and 29 with modifications to allow for swirl, forward flight and large induced flow angles. Although both variations produce similar results, the former was found to be more reliable at high forward flight speeds, while the latter performed better at zero and very low flight speeds. Both models used lookup tables for lift and drag obtained from the literature or using CFD. The Prandtl Glauert compressibility correction is utilized, but is capped at 0.7 Mach to avoid divergence. Flow interference factors were limited to 0.7 as suggested by Viterna and Janetzke.[30] Both models had the option of solving for a particular blade pitch angle, or converging to a known thrust or torque value. The latter was utilized to limit the introduction of aerodynamic error into the acoustic solution, however, its implementation generally had minimal impact. Validation of the BEMT implementation is not presented here, but good agreement was found for the thrust and torque distributions across a range of propeller geometries and operational conditions.

II.B. Acoustic Prediction

Three separate acoustic methods were implemented and used to produce the results presented in this paper. It should be noted that the noise was not simply evaluated at a given microphone location. To avoid complete noise cancellation between the thrust, torque and thickness terms, the noise was evaluated over a range of ±5 degrees relative to the original microphone location. The microphone position with the least destructive interference was then selected. This generally had a negligible impact on the acoustic signature of the propeller unless the loading or thickness terms were close in magnitude. The equations below give the root mean square pressure of the one-sided noise spectrum and are only valid for far-field noise. Near-field versions of these equations exist but were not implemented as they are outside the scope of this paper. The Sound Pressure Level (SPL) at a given harmonic was obtained using Eq. (1).

$$SPL_m = 20 \log \left(\frac{|P_{m_L} + P_{m_T}|}{P_0} \right) \tag{1}$$

Since the implemented noise models are readily available in the literature, only the main loading and thickness noise equations are presented here with comments regarding any modifications made in their implementation. The main equations are, however, described with enough detail for programming to increase the repeatability of the presented results.

Broadband noise models were initially implemented from the literature,[13] however, due to their negligible impact on the first few noise harmonic levels and their empirical nature,[8,21,31] they were later excluded from the results.

II.B.1. Coordinate System and Reference Frame

It is important to note that x, y, z, θ, ϕ, and S represent the physical distances and angles between the microphone or observer location and the propeller hub in a wind-tunnel configuration. In other words,

the listed variables are independent of forward Mach speed. This is equivalent to a moving-medium visual reference system. The equations by Gutin & Deming and by Barry & Magliozzi, were derived in a visual reference system, allowing direct implementation of the listed variables. Hanson's model, however, was derived in a retarded reference frame, meaning that a coordinate transformation is necessary before the method can be used. The coordinate transformations from a visual to a retarded reference frame required to implement Hanson's model are included below for clarity and are explained in detail in Refs. 32–34. The orientation of x, y, z is illustrated in Fig. 1, where x is positive in front of the propeller plane.

$$\cos\theta_r = \cos\theta\sqrt{1 - M^2\sin^2\theta} + M\sin^2\theta \tag{2}$$

$$S_r = \frac{Y}{\sin\theta_r} \tag{3}$$

II.B.2. Gutin and Deming

The first successful analytical acoustic theory was developed by Gutin, who modeled the steady aerodynamic forces acting on a propeller (torque and thrust) as a ring of dipole sources distributed over the propeller disc.[9] Following a similar procedure, Deming was the first to model the noise caused by finite blade thickness using the superposition of a continuous ring of sources and sinks in the propeller plane.[10,36] While not relevant for noise prediction in their original form to the majority of the selected validation cases, they were implemented to provide a baseline for the other two models.

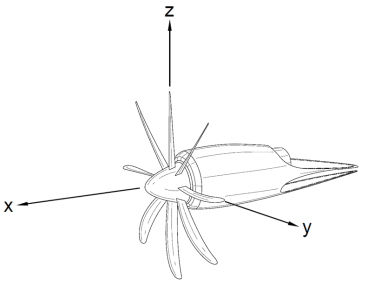

Figure 1. Coordinate axis orientation (adapted from Ref. 35).

The aforementioned formulations for loading and thickness noise are presented in Eq. (4) and Eq. (5). Discretized values for thrust and torque were used rather than the effective-radius approximation used by Gutin and Deming to maintain a consistent aerodynamic input across all prediction methods.

$$P_{m_L} = \frac{mB\Omega}{2\sqrt{2}\pi cS}\int_{hub}^{tip}\left[\frac{dT}{dR}\cos\theta - \frac{dQ}{dR}\frac{c}{\Omega R^2}\right]J_{mB}\left(\frac{mB\Omega}{c}R\sin\theta\right)dR \tag{4}$$

$$P_{m_T} = \frac{-\rho(mB\Omega)^2 B}{3\sqrt{2}\pi S}\int_{hub}^{tip} bhJ_{mB}\left(\frac{mB\Omega}{c}R\sin\theta\right)dR \tag{5}$$

Note that Eqs. (4) and (5) are limited to far-field predictions for propellers with no forward speed. This was rectified by the work of Garrick and Watkins[11] for loading noise and Arnoldi[12] for thickness noise.

II.B.3. Barry and Magliozzi

The equations of Garrick, Watkins, and Arnoldi for loading and thickness noise were further refined by Barry and Magliozzi to include the effect of blade twist to give Eqs. (6) and (7).[13] The alternate Bessel functions J_{mB+1} and J_{mB-1} appear because a more exact far field approximation was used by Barry and Magliozzi than is typically seen in the literature. Some phase terms have also been omitted because they do not alter the relative phase between loading and thickness noise. The absolute phase is not important for this application.

It should be noted that there are two differences between Eqs. (6) and (7) and the equations presented in Ref. 13. The first is a correction to the Bessel function term in both equations, as noted in Ref. 37. The second replaces $(1 - M^2)^4$ with $(1 - M^2)$ in the loading formulation. The latter makes Eq. (6) consistent with other forward flight formulations in the literature and avoids a large over-prediction of noise at higher forward Mach numbers.

$$P_{m_L} = \frac{1}{\sqrt{2}\pi S_0}\int_{hub}^{tip}\frac{R}{b\cos\phi_t}\sin\left(\frac{mBb\cos\phi_t}{2R}\right)\left[\frac{\big(M + X/S_0\big)\Omega}{c(1-M^2)}\frac{dT}{dR} - \frac{1}{R^2}\frac{dQ}{dR}\right]\left[J_{mB} + \frac{(1-M^2)YR}{2S_0^2}\big(J_{mB-1} - J_{mB+1}\big)\right]dR \tag{6}$$

$$P_{m_T} = -\frac{\rho m^2 \Omega^2 B^3}{2\sqrt{2}\pi(1-M^2)^2}\frac{(S_0+MX)^2}{S_0^3}\int_{hub}^{tip} A_x\left[J_{mB} + \frac{(1-M^2)YR}{2S_0^2}\big(J_{mB-1} - J_{mB+1}\big)\right]dR \tag{7}$$

$$J_{mB} = J_{mB}\left(\frac{mB\Omega YR}{cS_0}\right) \tag{8}$$

The equations derived by Garrick, Watkins, and Arnoldi can be retrieved by setting ϕ_t to zero, removing the alternate Bessel function terms (ie. seting J_{mB+1} and J_{mB-1} to zero) and replacing the sinusoid term in the loading equation by its argument.

II.B.4. Hanson

Hanson's formulation for loading and thickness noise extends the work of Garrick, Watkins, and Arnoldi to include the effects of non-compactness, sweep and non-axial flow.[8,14,15,34] The equations for loading and thickness noise are presented below, however, the reader is reminded that this formulation uses retarded coordinates. Any variables referring to the retarded reference frame are denoted by the subscript r.

$$P_{m_L} = \frac{imBM_t \sin\theta_r \exp\left[imB\left(\frac{\Omega S_r}{c} + (\phi' - \frac{\pi}{2})\right)\right]}{2\sqrt{2}\pi Y r_t(1 - M\cos\theta_r)}\int_{hub}^{tip}\left[\frac{\cos\theta_r'}{1-M\cos\theta_r}\frac{dT}{dr} - \frac{1}{r^2 M_t r_t}\frac{dQ}{dr}\right]\exp(i\phi_s)J_{mB}\Psi_L dr \tag{9}$$

$$P_{m_T} = \frac{-\rho c^2 B\sin\theta_r \exp\left[imB\left(\frac{\Omega S_r}{c} + (\phi' - \frac{\pi}{2})\right)\right]}{4\sqrt{2}\pi(Y/D)(1 - M\cos\theta_r)}\int_{hub}^{tip} M_s^2\big(h/b\big)\exp(i\phi_s)J_{mB}k_x^2\Psi_V dr \tag{10}$$

$$J_{mB} = J_{mB}\left(\frac{mBrM_t\sin\theta_r'}{1-M\cos\theta_r}\right) \tag{11}$$

where θ_r' and ϕ' relate to the angular flow angle, α, and are defined by:

$$\cos\theta_r' = \cos\theta_r\cos\alpha + \sin\theta_r\sin\phi\sin\alpha \tag{12}$$

$$\cos\phi' = \frac{\sin\theta_r}{\sin\theta_r'}\cos\phi \tag{13}$$

and k_x is a wave number given by:

$$k_x = \frac{2mBbM_t}{M_s(1-M\cos\theta_r)} \tag{14}$$

and ϕ_s represents phase lag due to sweep:

$$\phi_s = \frac{2mBM_t}{M_s(1-M\cos\theta_r)}\frac{MCA}{D} \tag{15}$$

Ψ_V and Ψ_L are non-dimensional source transforms which represent the effect of chord-wise non-compactness. A parabolic thickness distribution and uniform lift distribution, defined by Eq. (16) and Eq. (17) were used, as per Hanson's suggestion in Ref. 8. However, more exact forms can be employed if necessary.

$$\Psi_V(k_x) = \begin{cases} 2/3 & \text{if } k_x = 0, \\ \frac{8}{k_x^2}\left[\frac{2}{k_x}\sin(\frac{k_x}{2}) - \cos(\frac{k_x}{2})\right] & \text{if } k_x \neq 0. \end{cases} \tag{16}$$

$$\Psi_L(k_x) = \begin{cases} 1 & \text{if } k_x = 0, \\ \frac{2}{k_x}\sin(\frac{k_x}{2}) & \text{if } k_x \neq 0. \end{cases} \tag{17}$$

As noted by Hanson in Ref. 14, the above equations can be related back to earlier formulations by setting α to zero and with only minor modifications to the k_x argument of the source functions Ψ_V and Ψ_L. Arnoldi's thickness theory can be obtained by setting the k_x argument of Ψ_V to zero, while Garrick and Watkin's loading equations can be recovered by setting the argument of Ψ_L to mBb/R.

III. Selection of Validation Cases

Validation cases were selected such that they represented a wide range of propeller geometries and operating conditions. The following criteria were used in their selection:

1) Blade geometry and operating conditions were clearly defined.

2) Aerodynamic data, such as total thrust, was provided.

3) Multiple far-field microphone locations were used.

Fulfillment of the first criterion was required to implement the prediction models, the second ensured accuracy of the aerodynamic solvers and limited the introduction of aerodynamic error, while the third allowed for the evaluation of the capability of the acoustic models to predict directivity.

A large number of experiments were replicated in order to evaluate the flexibility of the implemented models and to mitigate the inconsistencies seen in some acoustic experiments.[22] A total of fourteen validation cases, summarized in Table 2, were selected for this paper, with nine from separate experiments. The propeller operational conditions and microphone locations of each test case are available in the references listed next to the authors in the table below. The propeller geometries are available from the same references with the exception of the SR-2, SR-3 and SR-7 propellers which were obtained from Refs. 22, 38 and 39, respectively. If additional aerodynamic data was used, separate from the reference listed next to the author, it is listed next to the propeller name.

Table 2. Experimental test cases selected for validation.

Test Case	Author	Year	Propeller	No. of Blades	Diameter (m)	Free Stream Mach No.	Helical Tip Mach No.
1	Soderman and Horne[22]	1990	SR-2	4	0.591	0.2	0.77
2	Dittmar[40]	1989	SR-2	8	0.622	0.6	0.86
3	Dittmar[40]	1989	SR-2	8	0.622	0.8	1.15
4	Dittmar and Jeracki[7]	1981	SR-3	8	0.622	0.5	0.72
5	Dittmar and Jeracki[7]	1981	SR-3	8	0.622	0.8	1.14
6	Dittmar and Stang[41]	1988	SR-7[42]	8	0.622	0.6	0.86
7	Dittmar and Stang[41]	1988	SR-7[42]	8	0.622	0.8	1.15
8	Brooks and Metzger[43]	1980	SR-3	2	0.648	0.2	0.78
9	Brooks and Metzger[43]	1980	SR-3	4	0.648	0.32	0.91
10†	Woodward[6]	1987	SR-7[44]	8	0.622	0.2	0.74
11	Hubbard[45]	1950	*	2	1.219	0.0	0.62
12	Brown and Ollerhead[46]	1971	Sensenich W60LK18	2	1.219	0.0	0.40
13	Brown and Ollerhead[46]	1971	W6 STD 8°	6	1.219	0.0	0.40
14	Dobrzynski et al.[47]	1986	F8475D-4	2	2.030	0.2	0.86

* propeller geometry included in Ref. 45

† provides acoustic data for non-axial flow

IV. Results

Results for each of the validation cases are presented in Figs. 2 to 11. Tone levels (SPL) are presented as a function of the angular position, θ, of the observer. Predictions are provided for the first and second harmonic for test cases 1, 2, 3 and 11, while results are provided for the first harmonic only for test cases 4–10, 12 and 13. A full spectrum of twenty harmonics is provided for test case 14 due to the fact that experimental data for only two microphones was available. No adjustments were made to any of the predicted results, with the exception of test cases 8 and 9 where corrected microphone locations where used as directed by the authors of the experiment.

It should also be noted that the results below have not been normalized to a constant sideline distance and represent a direct implementation of the experimental data from the literature. As such, Figs. 2 to 11 are not consistent in their representation of the distance between the observer and the microphone. The chosen format does, however, provide a compacts means of comparing unaltered experimental data to predictions from each acoustic model. The exact placement of transducers relative to the propeller is included in the appendix for every validation case.

Experimental data is not presented at some microphone locations due to experimental data not being available at those locations. This is occasionally due to transducer malfunction, but is more generally a result of the wind-tunnel background noise exceeding the propeller harmonic at that location.

IV.A. Test Case 1: Soderman and Horne

Acoustic results for test case 1, performed with a four-bladed NASA SR-2 propeller at a free stream Mach number of 0.2 and helical tip Mach number of 0.76, are shown in Fig. 2. SmartRotor and STAR-CCM+ failed to predict the second harmonic at the transducer nearest to the propeller axis.

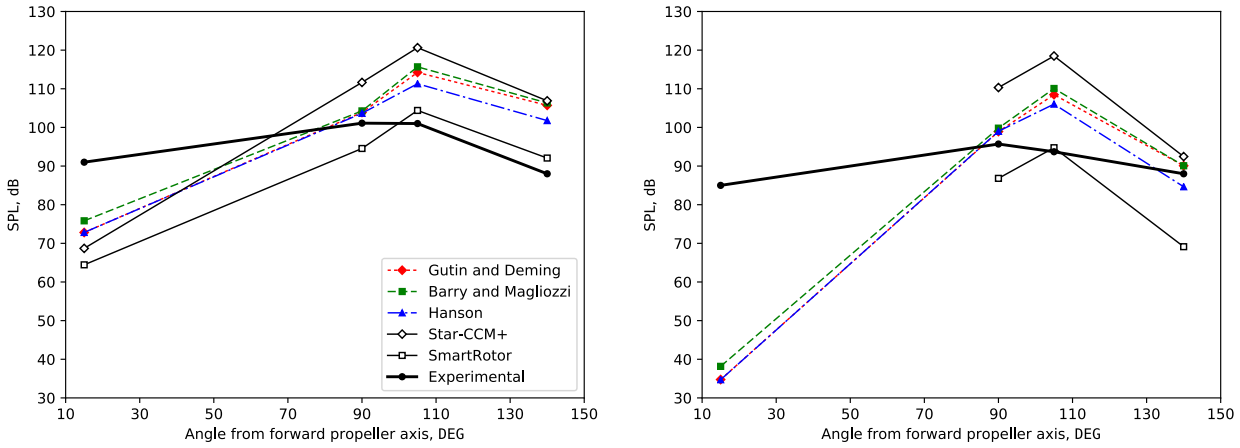

(a) First Harmonic.

(b) Second Harmonic.

Figure 2. Noise directivities - test case 1.

It is important to note that the microphones, whose locations are detailed in the appendix, are not at the same distance from the propeller hub. Transducer 7 and 8 are 1.4 meters from the hub, while transducers 9 and 12 are 2.4 and 4.3 meters from the hub, respectively. It is therefore unexpected that the experimentally measured noise at transducers 7 and 12 (positioned at an angular position of 105° and 90°) are almost identical. Reasons for this behavior are discussed by Soderman and Horne in Ref. 22.

IV.B. Test Case 2: Dittmar (M = 0.6)

Acoustic results for test case 2 are presented in Fig. 3. The second validation case uses similar propeller geometry as test case 1, but has eight blades and was performed at a forward Mach speed of 0.6, representative of cruise conditions.

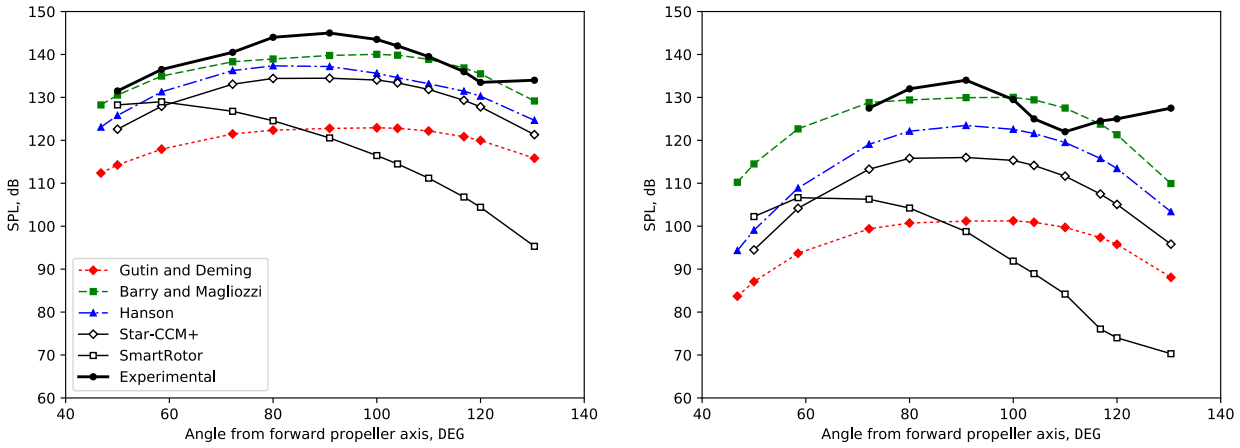

(a) First Harmonic. (b) Second Harmonic.

Figure 3. Tone directivities - test case 2.

IV.C. Test Case 3: Dittmar (M = 0.8)

Acoustic results for test case 3 are shown in Fig. 4. The propeller geometry is identical to test case 2 and differs only in the free stream Mach number and rotational speed. It should be noted that portions of the propeller undergo supersonic flow. For this reason, SmartRotor results are not presented, as the program is limited to the subsonic flow regime.

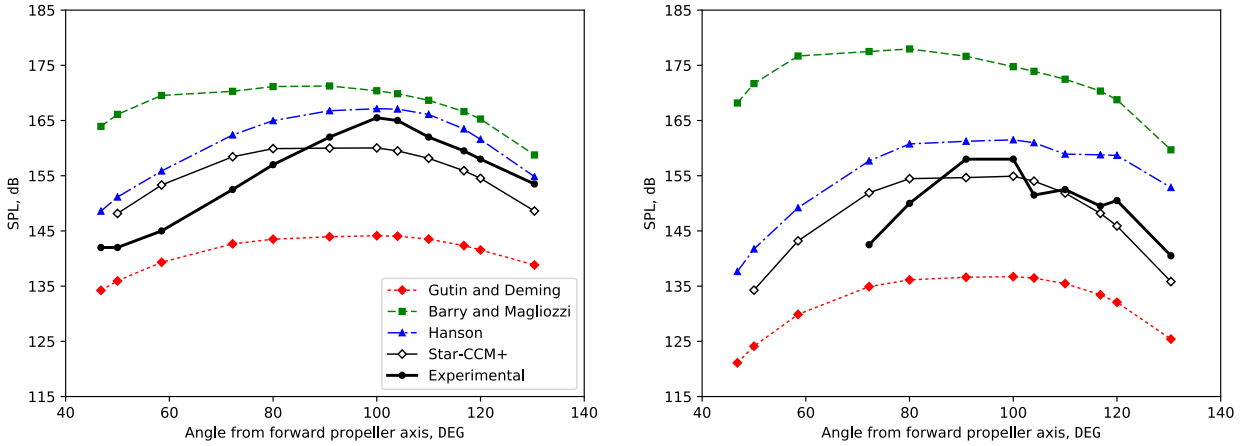

(a) First Harmonic. (b) Second Harmonic.

Figure 4. Tone directivities - test case 3.

IV.D. Test Case 4 and 5: Dittmar and Jeracki

Blade passing tone levels for test cases 4 and 5 are presented in Figs. 5a and 5b, respectively. Both utilize an eight-bladed SR-3 propeller and differ only in the free stream Mach number and rotational speed.

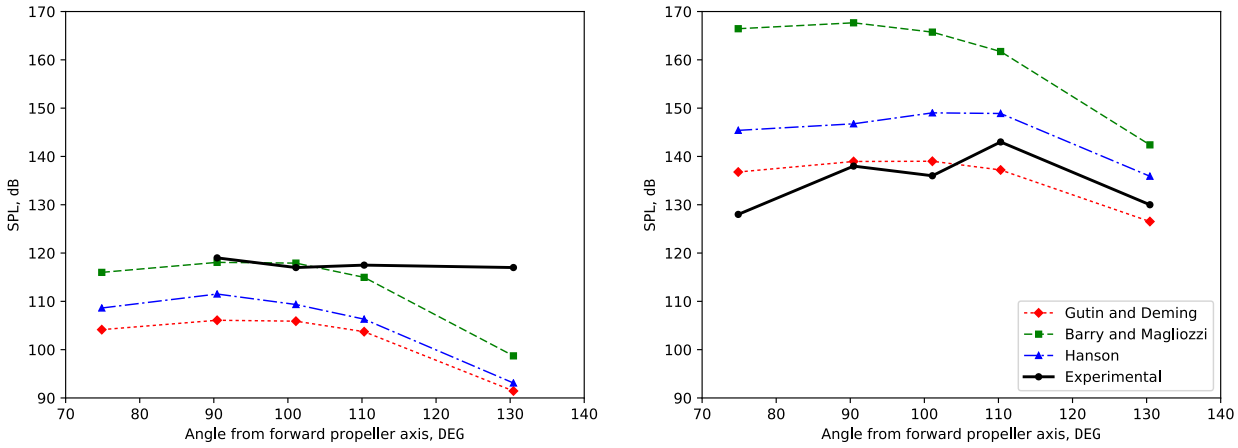

(a) M = 0.5. (b) M = 0.8.

Figure 5. Blade passing tone directivities - test cases 4 and 5.

IV.E. Test Case 6 and 7: Dittmar and Stang

Blade passing tone levels for test cases 6 and 7 are presented in Figs. 6a and 6b, respectively. Both utilize an eight-bladed SR-7 propeller and, again, differ only in the free stream Mach number and rotational speed.

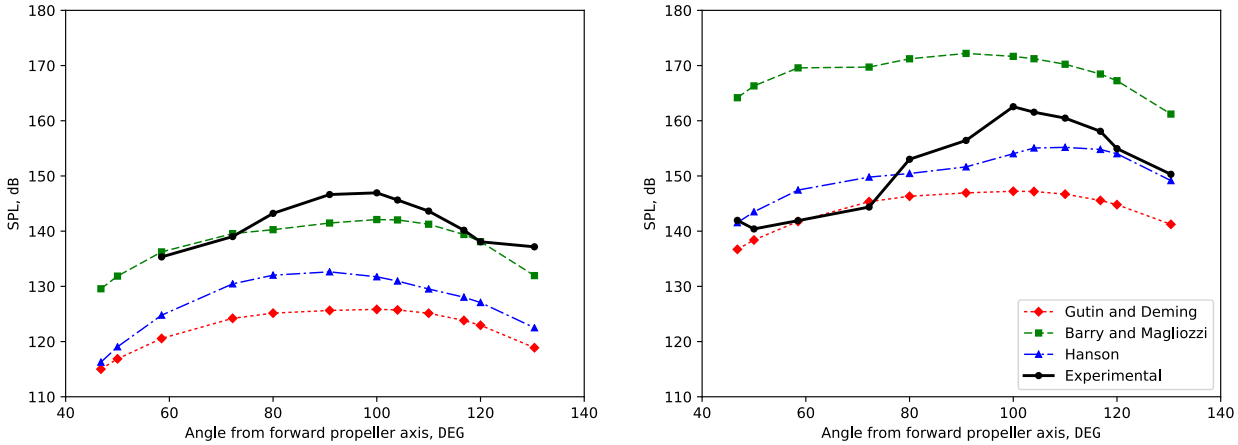

(a) M = 0.6. (b) M = 0.8.

Figure 6. Blade passing tone directivities - test cases 6 and 7.

IV.F. Test Case 8 and 9: Brooks and Metzger

Blade passing tone levels for test cases 8 and 9 are presented in Figs. 7a and 7b, respectively. An eight-blade configuration was not used for the SR-3 due to limitations in the power output of the propeller drive rig. Test case 8 is meant by the authors of the experiment to simulate takeoff and approach conditions, while test case 9 was performed to simulate cruise. Since the flight velocity of the wind-tunnel facility employed by Brooks and Metzger was limited to 0.32 Mach, the model was oversped to achieve a helical tip mach number representative of cruise conditions.[43]

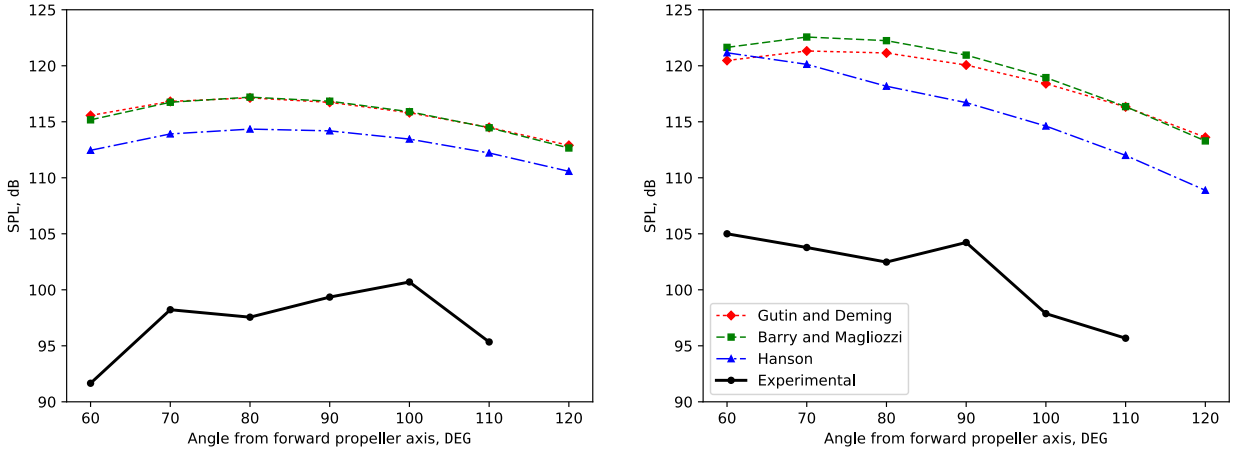

(a) M = 0.203, B = 2.

(b) M = 0.321, B = 4.

Figure 7. Blade passing tone directivities - test cases 8 and 9.

It should be noted that although results are plotted using the azimuth locations in Fig. 15a, they were produced using the corrected axial microphone locations, as described in the appendix. A discrepancy between the prediction models can be seen, even though the forward Mach speed is small, in part due to propeller sweep, which is only taken into account by Hanson's model.

IV.G. Test Case 10: Woodward

Blade passing tone levels for test case 10 are shown in Fig. 8. The experimental data obtained by Woodward, described in Ref. 6, specifically simulates takeoff and approach conditions and includes the effects of non-axial flow. Figure 8a corresponds to axial flow and serves as a baseline, while Fig. 8b presents data for a propeller with a positive 10 degree angle of attack. Results for a negative angle of attack are not presented here, but produced a similar yet opposite effect on the propeller acoustic signature. The significant difference between prediction methods is, again, in part due to sweep.

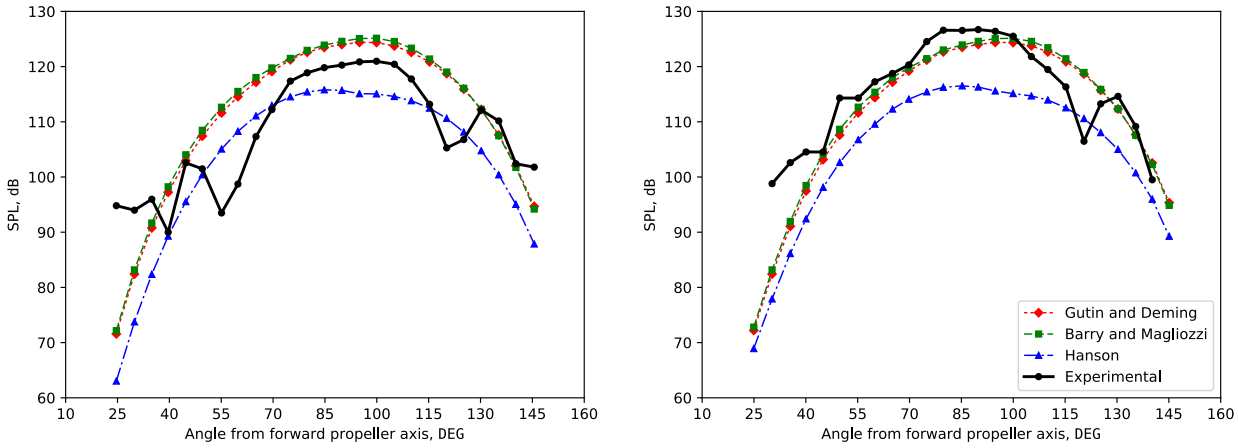

(a) $\alpha = 0°$.

(b) $\alpha = 10°$ (positive pitch angle).

Figure 8. Blade passing tone directivities - test case 10.

IV.H. Test Case 11: Hubbard

Acoustic results for the blade passing frequency and second harmonic of test case 11 are given in Fig. 9. Experimental data for test case 11 was obtained using an outdoor static test stand and a two-bladed propeller. The geometry of the propeller is given in Ref. 45.

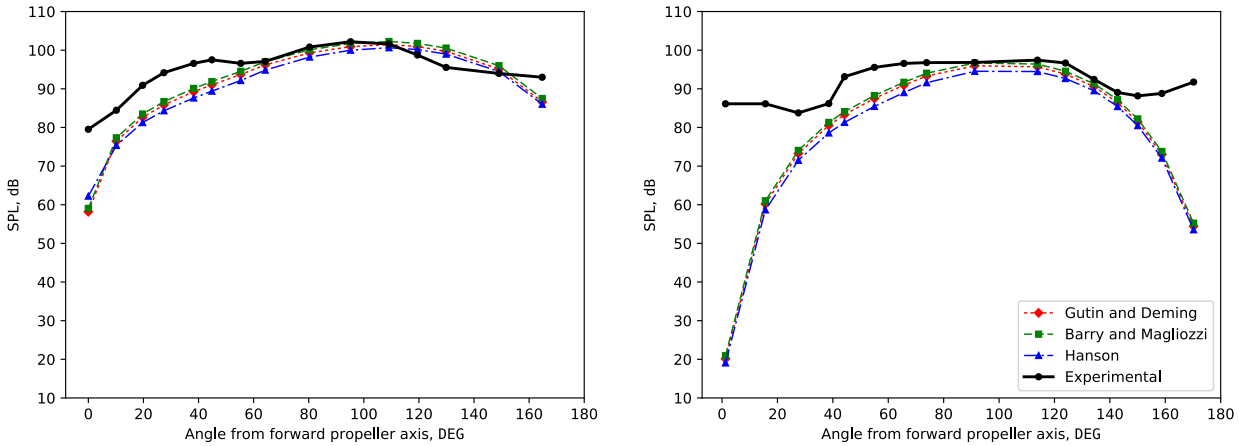

(a) First Harmonic.

(b) Second Harmonic.

Figure 9. Tone directivities - test case 11.

IV.I. Test Case 12 and 13: Brown and Ollerhead

Blade passing tone levels for test cases 12 and 13 are presented in Figs. 10a and 10b, respectively. Both test cases were performed under static conditions, but differ in blade geometry and number. The geometry of each propeller is provided in Ref. 43. It is interesting to note that the experimental data remains relatively constant regardless of the observer angle for both test cases 12 and 13, but decreases significantly near the axis for test case 11. This may be due to the lower blade loading in test cases 12 and 13, where unaccounted sources of noise may be dominant.

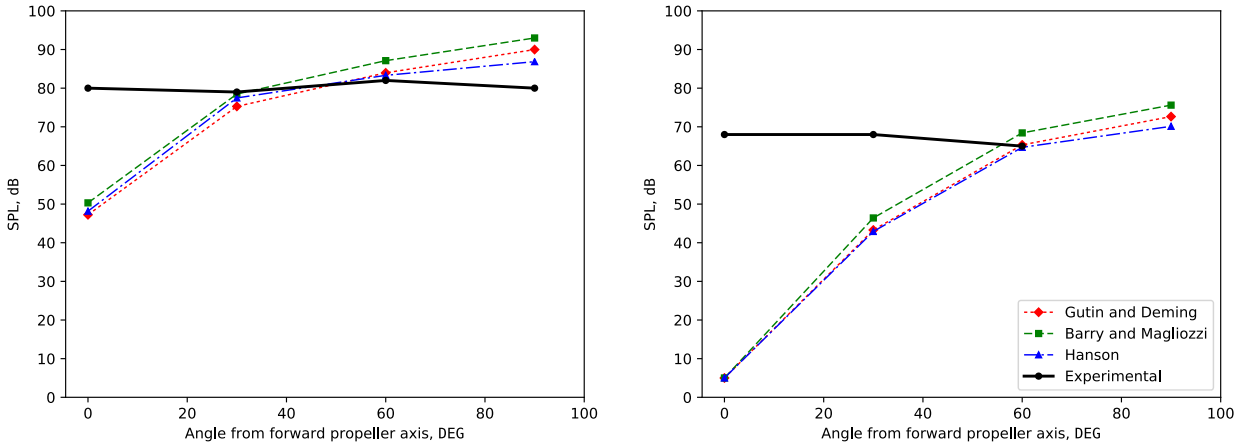

(a) Sensenich propeller, B = 2.

(b) W6 STD 8° propeller, B = 6.

Figure 10. Blade passing tone directivities - test cases 12 and 13.

IV.J. Test Case 14: Dobrzynski et al.

The harmonic noise spectra of test case 14, performed with a full-scale two-bladed propeller at a free stream Mach number of 0.2 and helical tip Mach number of 0.86, is shown in Fig. 11. Only two microphone locations (microphones 4 and 5) were considered due to the fact that data for other transducer locations was not readable from the source document. Since data for only two transducer positions was available, the harmonic spectrum of the first twenty harmonics was plotted instead. The agreement with the experiment up to the twentieth harmonic is unexpected as Gutin and Deming's noise formulations are known to only be accurate at low order harmonics.[20,46]

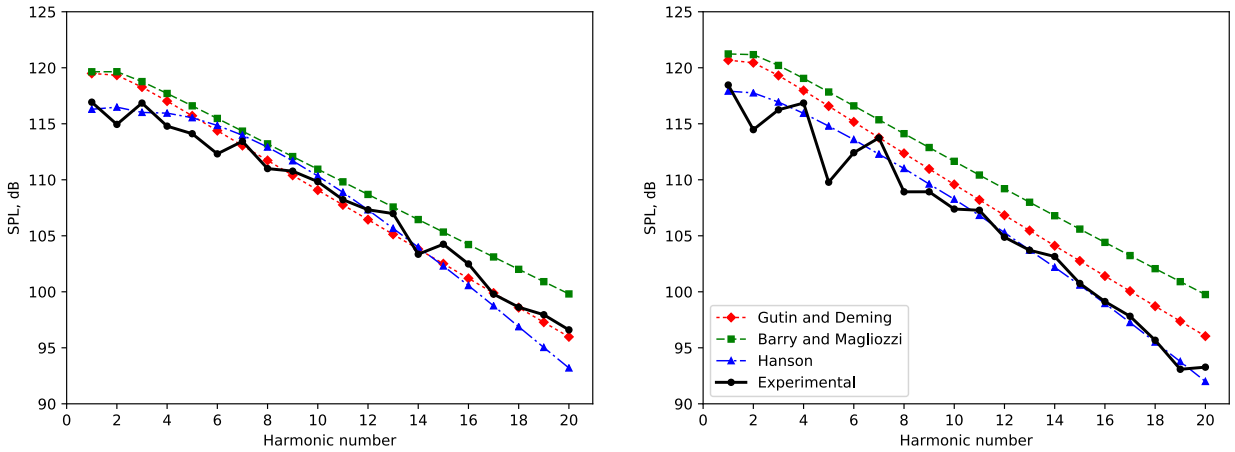

(a) Transducer 4.

(b) Transducer 5.

Figure 11. Noise spectra - test case 14.

IV.K. Results Summary

Acoustic prediction accuracy of each noise model for every test case is presented in Table 3. The non-bracketed term qualifies the capability of the models in predicting the maximum noise level and usually corresponds to the prediction error of transducers near the propeller plane. The term in brackets, on the other hand, is a measure of the consistency of the models at different transducer locations and typically matches the prediction error at the transducer closest to the propeller axis. From Table 3, it can be seen that Hanson's model outperforms the other prediction methods with an average 7.2 dB over-prediction or under-prediction of the maximum sound pressure level. The performance of Hanson's model relative to the noise formulations by Gutin & Deming and Barry & Magliozzi was expected, being a more recent and advanced formulation. The poor accuracy of SmartRotor and StarCMM+, however, was unexpected and is inconsistent with the accuracy associated with these methods presented in the literature. Independent of individual validation cases, some general trends were observed:

1) Experimental and predicted results varied significantly across test cases and microphone locations, emphasizing the need for thorough validation of acoustic models with multiple test cases and a range of microphone positions being considered.

2) Better acoustic predictions were obtained near the propeller plane, with poor accuracy near the axis.

3) The formulations by Gutin and Deming showed good agreement with experiment up to freestream velocities of 0.3 Mach.

4) The formulations by Barry and Magliozzi showed good agreement with experiment up to freestream velocities of 0.6 Mach.

5) The formulations by Hanson generally under-predicted the noise of low-speed, swept propellers, with the exception of test cases 8 and 9.

6) The implementation of non-axial flow into Hanson's model using Refs. 15 and 34 had limited success as angle of attack was found to have only a minor impact on the predicted noise signature of the propeller. This can likely be attributed to the fact that only steady loading was considered.

7) Acoustic data obtained using SmartRotor significantly under-predicted the noise relative to other methods. The prediction behavior of SmartRotor in Fig. 3 suggests that there may have been an error in its implementation.

8) Acoustic data obtained using STAR-CCM+ showed substantial variation across test cases, but showed the least variance over the available transducers in each test case, with an average maximum error of 22.9 dB.

Results for the validation cases presented suggest that acoustic models based on the work of Gutin and Deming and particularly the formulations derived by Hanson provide a good first estimate for propeller noise. All three methods were observed to have lower error relative to data obtained with a panel method and grid-based CFD method coupled to the FW-H equation. This is not to suggest that methods based on the FW-H equation are generally less accurate than the implemented methods, however, the above results demonstrate the capability of early acoustic methods for the prediction of far-field, propeller-alone harmonic noise across a range of propeller configurations, including the modern, high speed prop-fan.

Table 3. Summary of acoustic model performance.

Test Case	Harmonic	Error at location of maximum noise*, dB (Maximum error†, dB)				
		Gutin and Deming	Barry and Magliozzi	Hanson	SmartRotor	STAR-CCM+
1	1	13.1 (-18.2)	14.6 (18.3)	10.2 (-18.2)	3.29 (-26.6)	19.5 (-22.3)
	2	12.8 (-50.3)	14.4 (-46.8)	10.3 (-53.3)	-0.95 (-18.9)	22.8 (24.8)
2	1	-22.1 (-22.2)	-4.97 (-5.23)	-7.65 (-9.34)	-16.0 (-38.7)	-10.5 (-12.7)
	2	-32.8 (-39.4)	-4.00 (-17.6)	-10.5 (-24.1)	-27.4 (-57.2)	-18.0 (-31.7)
3	1	-21.4 (-21.4)	5.76 (24.5)	1.64 (10.9)	-	-5.47 (8.32)
	2	-21.3 (-21.4)	20.0 (35.0)	3.50 (15.2)	-	-3.09 (9.41)
4	1	-12.9 (-25.6)	-0.931 (-18.3)	-7.48 (-23.9)	-	-
5	1	-4.00 (8.78)	24.7 (38.4)	6.02 (17.4)	-	-
6	1	-21.1 (-21.1)	-4.84 (-5.21)	-14.3 (-15.2)	-	-
7	1	-15.3 (-15.3)	9.65 (27.7)	-7.37 (-8.52)	-	-
8	1	16.4 (23.9)	16.5 (23.5)	13.7 (20.8)	-	-
9	1	16.3 (20.7)	17.6 (21.1)	16.2 (16.7)	-	-
10‡	1	3.41 (-23.2)	4.16 (-22.6)	-5.18 (-31.8)	-	-
	1	-2.32 (-16.4)	-1.58 (-15.6)	-10.2 (-20.9)	-	-
11	1	-0.737 (-21.3)	0.068 (-20.5)	-1.56 (-17.3)	-	-
	2	-1.48 (-66.0)	-0.765 (-65.2)	-2.89 (-67.0)	-	-
12	1	7.99 (-32.8)	11.0 (-29.7)	4.86 (-31.8)	-	-
13	1	4.65 (-63.0)	7.61 (-63.0)	2.12 (-63.0)	-	-
14	1	1.67 (1.67)	2.23 (2.23)	-1.09 (-1.71)	-	-
Avg.§	-	12.2 (27.0)	8.70 (26.3)	7.20 (24.6)	11.9 (25.0)	14.8 (22.9)

* difference between maximum experimental and maximum predicted noise; locations of maximum noise are not necessarily identical between experimental and predicted results

† maximum error between experimental and predicted data across all transducer locations

‡ error for axial flow is presented first, followed by non-axial flow

§ the modulus of the error values is taken before averaging

V. Conclusions

Three different acoustic prediction methods based on early acoustic theory were implemented from the literature and validated against fourteen test cases. Acoustic data was also obtained using a panel method (SmartRotor) and a grid-based CFD method (STAR-CCM+) coupled to the FW-H equation to compare the relative accuracy of the frequency-domain methods for a limited number of test cases. The implemented methods only required easily obtainable geometric and operational data and used blade element momentum theory to approximate the radial thrust and torque distributions. The selected test cases ranged in propeller configuration and operational conditions to characterize the limits of the prediction methods. A substantial number of validation cases were used in an effort to identify the general behavior of each prediction method and limit the influence of inconsistencies within the predicted and experimental results.

The acoustic predictions showed significant variation in accuracy across test cases and at different microphone locations, highlighting the need for multiple test cases to be considered in the validation of acoustic models. Nevertheless, noise comparisons of the implemented acoustic models showed good agreement with experiment and each implemented method demonstrated better accuracy than both methods coupled to the FW-H equation. Hanson's model was the most consistent and accurate of the evaluated methods, with an average error of 7.2 dB in the maximum tonal noise relative to experiment. The presented results indicate the potential of early acoustic methods, particularly for design and optimization studies, and demonstrate their relevance for the noise prediction of modern, high speed, prop-fan configurations.

Appendix

The positions of the microphones in the experiments selected for validation are described below. The circled microphones in Figs. 12 and 17 represent microphones for which valid experimental data was available. Those circled in Fig. 12 represent locations for which propeller-alone or propeller-fuselage data was available. Acoustic data for the other microphone locations was only available with the aircraft tail present in the wind-tunnel, which alters the harmonic SPL and is therefore not used for comparison. The fuselage itself was shown by Soderman and Horne to have negligible impact on the harmonic sound level.[22] Only microphones 4 and 5 were used in test case 14 (circled in red in Fig. 17) as data for the other microphones was illegible from the source document.

The microphone positions of test cases 8 and 9 were adjusted using Fig. 3-5 from Ref. 43 to correct for tunnel shear layer effects as directed by Brooks and Metzger. This correction factor translates to a shift in the axial microphone position that is described by Fig. 15b. A third order polynomial fit of the curve defined in Fig. 15b was used such that $x_c = 0.0229x^3 - 0.149x^2 + 0.927x - 0.834$, where x_c is the corrected axial location used to produce results for test cases 8 and 9.

The translating microphone probe used in test case 10, depicted in Fig. 16, is in plane with the propeller axis and maintains a sideline distance of 1.68 meters.

The microphone positions for test case 11 were distributed along an arc 9.14 meters from the propeller hub (30 feet). The microphones in test cases 12 and 13 were positioned along an arc 3.66 meters (12 feet) from the hub at azimuth locations of 0°, 30°, 60° and 90°. In both experiments, the observer angle is taken relative to the forward propeller axis and the microphones are assumed to be in plane with the propeller axis ($z = 0$).

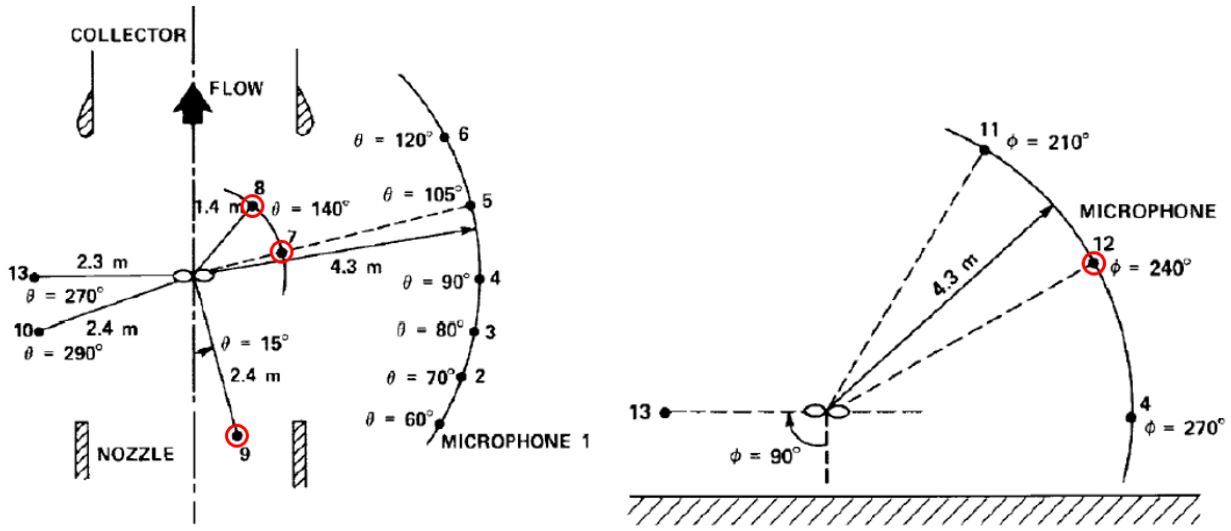

(a) Top view.

(b) Front view looking downstream at the propeller plane.

Figure 12. Microphone locations relative to propeller hub - test case 1 (from Ref. 22).

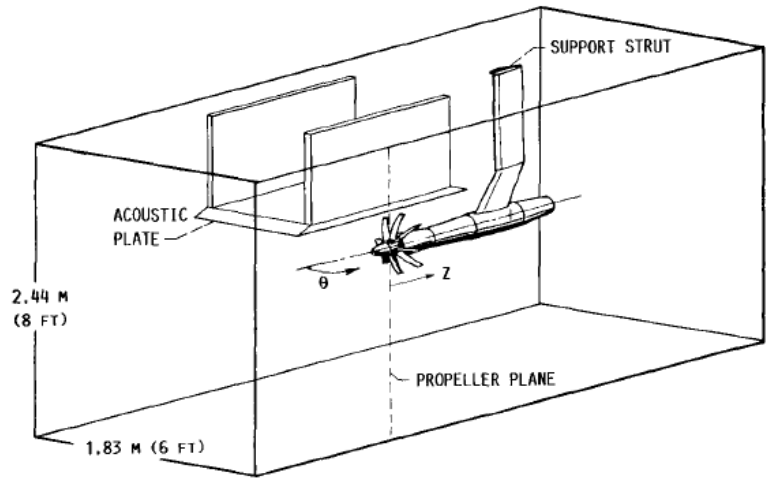

TRANSDUCER (PLATE 0.3 DIAMETER FROM TIP)											
1	2	3	4	5	6	7	8	9	10	11	12
TRANSDUCER DISTANCE FROM PROPELLER PLANE, Z, CM (IN.)											
-46.7 (-18.4)	-41.7 (-16.4)	-30.5 (-12.0)	-16.0 (-6.3)	-8.9 (-3.5)	0.8 (0.3)	8.9 (3.5)	12.4 (4.9)	18.0 (7.1)	25.0 (9.9)	28.7 (11.3)	42.4 (16.7)
ANGLE FROM UPSTREAM, θ, DEG											
46.8	50.0	58.5	72.2	80	90.9	100	104	110	116.8	120	130.4

Figure 13. Microphone locations - test cases 2, 3, 6 and 7 (from Ref. 40).

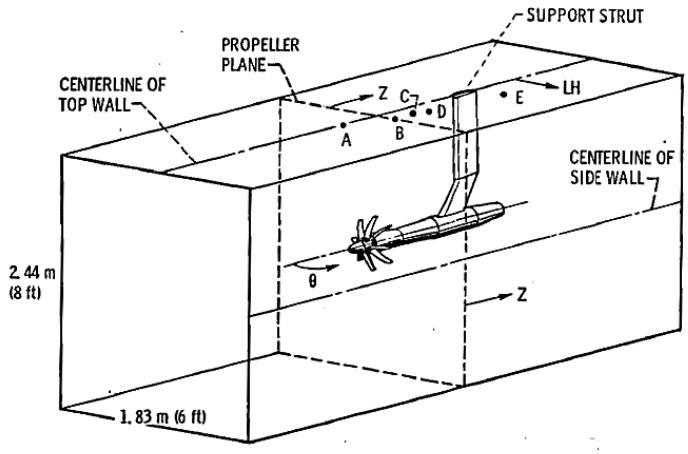

POSITION	TRANSDUCER				
	A	B	C	D	E
	TRANSDUCER POSITION, cm (in.)				
Z LH	33.0(13.0) 4.83(1.9)	0.953(0.375) 10.2(4.0)	23.9(9.4) 2.54(1.0)	45.2(17.8) 7.62(3.0)	107.4(42.3) 31.5(12.4)
NOMINAL ANGLE, θ, deg.	75	90	101	110	131

Figure 14. Microphone locations - test cases 4 and 5 (from Ref. 7).

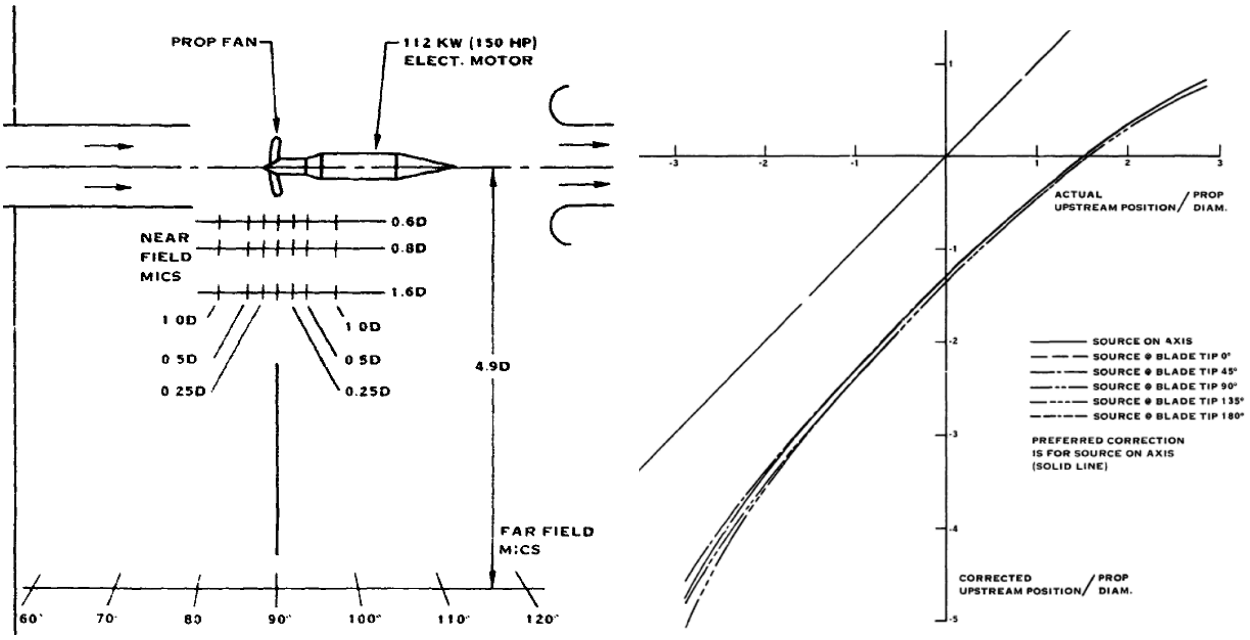

(a) Microphone locations. (b) Axial correction factor.

Figure 15. Microphone locations and axial correction factor - test cases 8 and 9 (from Ref. 43).

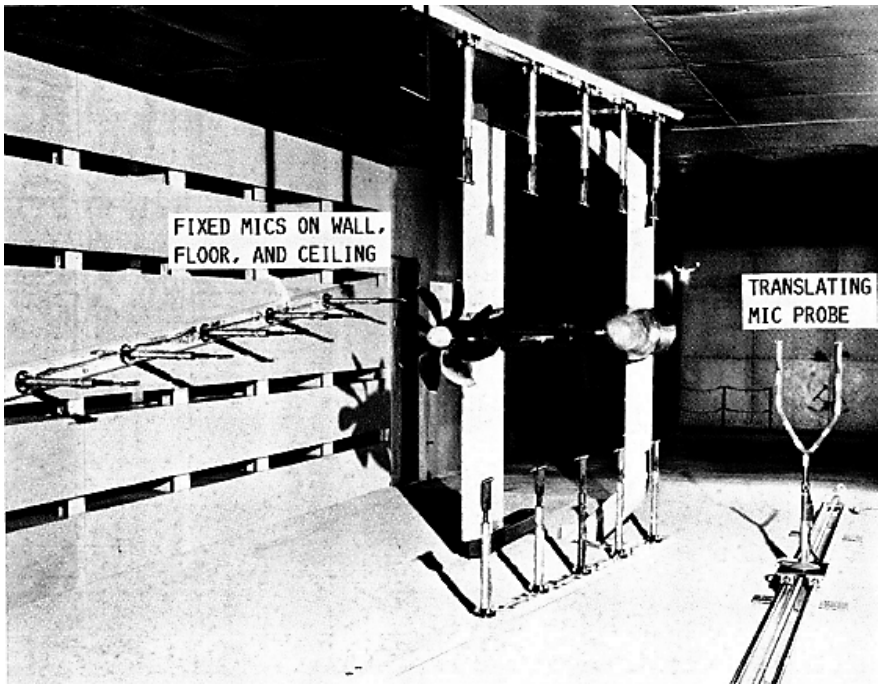

Figure 16. Microphone locations - test case 10 (from Ref. 6).

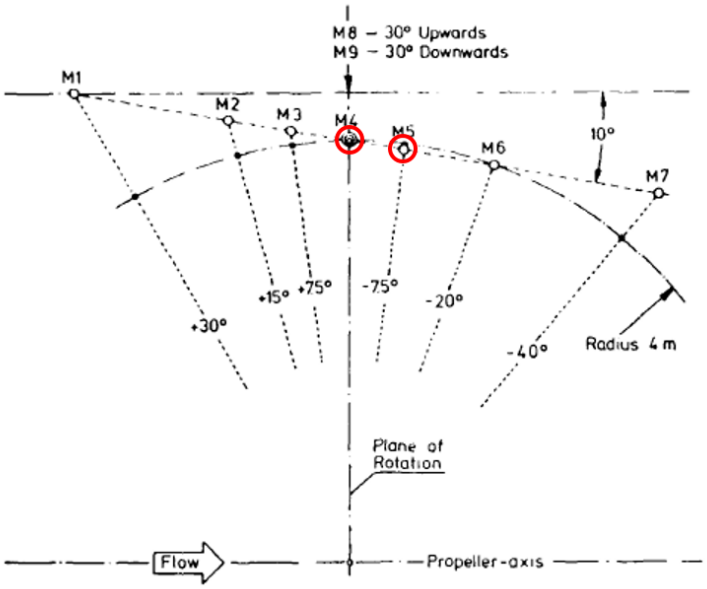

Figure 17. Microphone locations - test case 14 (from Ref. 47).

Acknowledgments

This work was pursued in collaboration with Pratt & Whitney Canada and was supported by the Green Aviation Research and Development Network (GARDN).

References

[1]Peterson, R., "Regional Turboprop Resurgence Continues; Jet Demand Shifts Upward," *Aircraft Engineering and Aerospace Technology*, Vol. 80, No. 2, 2004.

[2]Ryerson, M. S. and Hansen, M., "The potential of turboprops for reducing aviation fuel consumption," *Transportation Research Part D: Transport and Environment*, Vol. 15, No. 6, 2010, pp. 305–314.

[3]Holsclaw, C., "Stage 5 Airplane Noise Standards," 81 FR 1923, Federal Aviation Administration, Washington, DC, Jan. 2016.

[4]Franssen, E., van Wichen, C., Nagelkerke, N., and Lebret, E., "Aircraft noise around a large international airport and its impact on general health and medication use," *Occupational and Environmental Medicine*, Vol. 61, No. 5, 2004, pp. 405–413.

[5]Swift, H., "A Review of the Literature Related to Potential Health Effects of Aircraft Noise," PARTNER-COE-2010-003, Partnership for Air Transportation Noise and Emissions Reduction, Cambridge, MA, July 2010.

[6]Woodward, R. P., "Measured Noise of a Scale Model High Speed Propeller at Simulated Takeoff/Approach Conditions," NASA-TM-88920, Lewis Research Center, Cleveland, OH, Jan. 1987.

[7]Dittmar, J. H. and Jeracki, R. J., "Additional Noise Data on the SR-3 Propeller," NASA-TM-81736, Lewis Research Center, Cleveland, OH, May 1981.

[8]Magliozzi, B., Hanson, D. B., and Amiet, R. K., "Propeller and Propfan Noise," *Aeroacoustics of Flight Vehicles: Theory and Practice*, edited by H. H. Hubbard, Vol. 1, NASA, Hampton, VA, 1991, pp. 1–61.

[9]Gutin, L., "On the sound field of a rotating propeller," NACA-TM-1195, National Advisory Committee for Aeronautics, Washington, DC, Oct. 1948.

[10]Deming, A. F., "Noise from Propellers with Symmetrical Sections at Zero Blade Angle II," NACA-TN-679, National Advisory Committee for Aeronautics, Washington, DC, Dec. 1938.

[11]Garrick, I. E. and Watkins, C. E., "A Theoretical Study of the Effect of Forward Speed on the Free-Space Sound-Pressure Field Around Propellers," NACA-TN-3018, National Advisory Committee for Aeronautics, Washington, DC, Oct. 1953.

[12]Arnoldi, R. A., "Propeller Noise Caused by Blade Thickness," R-0896-1, United Aircraft Corporation Research Department, East Hartford, CT, Jan. 1956.

[13]Barry, F. W. and Magliozzi, B., "Noise Detectability Prediction Method for Low Tip Speed Propellers," AFAPL-TR-71-37, Hamilton Standard, Wright-Patterson Air Force Base, OH, June 1971.

[14]Hanson, D. B., "Helicoidal Surface Theory for Harmonic Noise of Propellers in the Far Field," *AIAA Journal*, Vol. 18, No. 10, 1980, pp. 1213–1220.

[15]Hanson, D. B., "Sound from a Propeller at Angle of Attack: A New Theoretical Viewpoint," *Proceedings: Mathematical and Physical Sciences*, Vol. 449, No. 1936, 1995, pp. 315–328.

[16]Ffowcs Williams, J. E. and Hawkings, D. L., "Sound Generation by Turbulence and Surfaces in Arbitrary Motion," *Philosophical Transactions of the Royal Society of London. Series A, Mathematical and Physical Sciences*, Vol. 264, No. 1151, 1969, pp. 321–342.

[17]Farassat, F., "Derivation of Formulations 1 and 1A of Farassat," NASA-TM-2007-214853, Langley Research Center, Hampton, VA, March 2007.

[18]Morfey, C. L., "Rotating blades and aerodynamic sound," *Journal of Sound and Vibration*, Vol. 28, No. 3, 1973, pp. 587–617.

[19]Magliozzi, B., Metzger, F. B., Baush, W., and King, R. J., "A Comprehensive Review of Helicopter Noise Literature," FAA-RD-75-79, Federal Aviation Administration, Washington, DC, June 1975.

[20]Farassat, F. and Succi, G. P., "A review of propeller discrete frequency noise prediction methodology with emphasis on two current methods for time domain calculations," *Journal of Sound and Vibration*, Vol. 71, No. 3, 1980, pp. 399–419.

[21]Metzger, B., "A review of propeller noise prediction methodology: 1919-1994," NASA-CR-198156, Langley Research Center, Hampton, VA, June 1995.

[22]Soderman, P. T. and Horne, W. C., "Acoustic and Aerodynamic Study of a Pusher-Propeller Aircraft Model," NASA-TP-3040, Ames Research Center, Moffet Field, CA, Sept. 1990.

[23]Boots, D., *Numerical predictions of propeller-wing interaction induced noise in cruise and off-design conditions*, Master's thesis, Carleton University, Ottawa, ON, Aug. 2016.

[24]Nitzsche, F. and Opoku, D. G., "Acoustic Validation of a New Code Using Particle Wake Aerodynamics and Geometrically-Exact Beam Structural Dynamics," *The Aeronautical Journal*, Vol. 109, No. 1096, 2005, pp. 257–267.

[25]Hambrey, J., *Computational Aeroacoustic Prediction of Propeller Noise Using Grid-Based and Grid-Free CFD Methods*, Master's thesis, Carleton University, Ottawa, ON, Aug. 2016.

[26]Hambrey, J. R., Kotwicz Herniczek, M. T., Feszty, D., Meslioui, S., and Park, J., "Comparison of Three Popular Methods for the Prediction of High Speed Propeller Noise," *Proceedings of the 23rd AIAA/CEAS Aeroacoustics Conference*, AIAA, Denver, CO, 2017.

[27]Atkins, C. N. and Leibeck, R. H., "Design of Optimum Propellers," *Journal of Propulsion and Power*, Vol. 10, No. 5, 1994, pp. 676–682.

[28]Leishman, G., *Principles of Helicopters Aerodynamics*, Cambridge University, New York, 2006.

[29]Hodges, D. H., "An Extension of Blade Element Momentum Theory to Incorporate Nonlinear Lift and Drag Coefficients," *Journal of the American Helicopter Society*, Vol. 25, No. 4, 1981, pp. 48–50.

[30]Viterna, L. A. and Janetzke, D. C., "Theoretical and Experimental Power from Large Horizontal-Axis Wind Turbines," NASA-TM-82944, Lewis Research Center, Cleveland, OH, Sept. 1982.

[31]Marte, J. E. and Kurtz, D. W., "A Review of Aerodynamic Noise From Propellers, Rotors and Lift Fans," NASA-TR 32-1462, California Institute of Technology, Pasadena, CA, Jan. 1970.

[32]Hanson, D. B., "Influence of Propeller Design Parameters on Far-Field Harmonic Noise in Forward Flight," *AIAA Journal*, Vol. 18, No. 11, 1980, pp. 1313–1319.

[33]Jacques, J., "Wind-tunnel Simulation of the Effects of Flight on Radiated Sound," C.P. No. 1351, Aeronautical Research Council, London, England, 1976.

[34]Hanson, D. B. and Parzych, D. J., "Theory for Noise of Propellers in Angular Inflow With Parameteric Studies and Experimental Verification," NASA-CR-4499, Hamilton Standard, Windsor Locks, CT, March 1993.

[35]Saint-Jalmes, B., Zaneboni, J., and Rumeau, B., "Engine nacelle with propeller," U.S. Patent D633429 S1, 2009.

[36]Deming, A. F., "Propeller Rotation Noise Due to Torque and Thrust," *Journal of the Acoustical Society of America*, Vol. 12, No. 1, 1940, pp. 173–182.

[37]Griffith, E. D. and Revell, J. D., "Low Noise Propeller Technology Demonstration," AFA1L-TR-73-115, Lockheed-California Company, Burbank, CA, Jan. 1974.

[38]Billman, L. C., Ladden, R. M., Turnberg, J. E., Gruska, C. J., and Leishman, D. K., "Large Scale Prop-fan Structural Design Study: Volume II - Preliminary Design of SR-7," NASA-CR-174993, Hamilton Standard, Washington, DC, Aug. 1989.

[39]Stefko, G. L., Rose, G. E., and Podboy, G. G., "Wind Tunnel Performance Results of an Aeroelastically Scaled 2/9 Model of the PTA Flight Test Prop-Fan," NASA-TM-89917, Lewis Research Center, Cleveland, OH, July 1987.

[40]Dittmar, J. H., "Cruise Noise of the SR-2 Propeller Model in a Wind Tunnel," NASA-TM-101480, Lewis Research Center, Cleveland, OH, April 1989.

[41]Dittmar, J. H. and Stang, D. B., "Cruise Noise of the 2/9 Scale Model SR-7A Propeller," *Journal of Aircraft*, Vol. 25, No. 8, 1988, pp. 740–746.

[42]Parzych, D., Cohen, S., and Shenkman, A., "Large-Scale Advanced Propfan (LAP) Performance, Acoustic and Weight Estimation," NASA-CR-174782, Hamilton Standard, Washington, DC, Feb. 1985.

[43]Brooks, B. M. and Metzger, F. B., "Acoustic Test and Analysis of Three Advanced Turboprop Models," NASA-CR-159667, Hamilton Standard, Windsor Locks, CT, Jan. 1980.

[44]Nallasamy, M., Woodward, R. P., and Groeneweg, J. F., "High-Speed Propeller Performance and Noise Predictions at Takeoff/Landing Conditions," *Journal of Aircraft*, Vol. 26, No. 6, 1989, pp. 563–569.

[45]Hubbard, H. H., "Sound Measurements for Five Shrouded Propellers at Statics Conditions," NACA-TN-2024, Langley Aeronautical Laboratory, Cleveland, OH, April 1950.

[46]Brown, D. and Ollerhead, J. B., "Propeller Noise at Low Tip Speeds," AFAPL-TR-71-55, Wyle Laboratories, Hampton, VA, Sept. 1971.

[47]Dobrzynski, W. M., Heller, H. H., Powers, J. O., and Densmore, J. E., "Propeller Noise Tests in the German-Dutch Wind Tunnel DNW," Report No. AEE 86-3, Federal Aviation Administration, Washington, DC, Dec. 1986.